

Channel-Partitioned Windowed Attention And Frequency Learning for Single Image Super-Resolution

Dinh Phu Tran
phutx2000@kaist.ac.kr

Korea Advanced Institute of
Science and Technology
Daejeon, Korea

Dao Duy Hung
nicehehe@kaist.ac.kr

Daeyoung Kim
kmd@kaist.ac.kr

arXiv:2407.16232v1

Abstract

Recently, window-based attention methods have shown great potential for computer vision tasks, particularly in Single Image Super-Resolution (SISR). However, it may fall short in capturing long-range dependencies and relationships between distant tokens. Additionally, we find that learning on spatial domain does not convey the frequency content of the image, which is a crucial aspect in SISR. To tackle these issues, we propose a new Channel-Partitioned Attention Transformer (CPAT) to better capture long-range dependencies by sequentially expanding windows along the height and width of feature maps. In addition, we propose a novel Spatial-Frequency Interaction Module (SFIM), which incorporates information from spatial and frequency domains to provide a more comprehensive information from feature maps. This includes information about the frequency content and enhances the receptive field across the entire image. Experimental findings demonstrate the effectiveness of our proposed modules and architecture. In particular, CPAT surpasses current state-of-the-art methods by up to **0.31dB**.

1 Introduction

Single Image Super-Resolution (SISR) is a low-level vision task that aims to enhance a low-resolution (LR) image into a high-resolution (HR) image.

Initially, convolutional neural networks [26, 27, 28, 31, 32] achieved outstanding results in SISR a few years ago. However, it does not possess the capability to gather global contextual information, as they mainly focus on nearby areas and might miss out on important connections that are far apart. Recently, Transformers, which utilize self-attention mechanisms, excel at modeling long-range dependencies not only with high-level vision tasks such as Image Captioning [29, 30], 3D-aware Image Synthesis [33], etc., but also with low-level vision tasks such as localization [34], segmentation [35, 36], etc., including SISR [37, 38, 39, 40].

Although Transformer has shown great performance in SISR compared to CNN-based methods, they still have limitations that need to be dealt with. The use of dense attention

in IPT [2] focuses on short token sequences that come from a dense area of an image. As a result, the receptive field is restricted due to this approach. SwinIR [32] employs a Swin Transformer as the main backbone, which has a main drawback is that it limits the receptive fields for extracting information from global information. Although HAT [10] is state-of-the-art in SISR, it still uses Swin Transformer, thus limiting the extraction of global information. Therefore, the current methods still can not fully exploit the potential of Transformer for SISR. On the other hand, current methods in SISR mainly extract features from the spatial domain without leveraging features extracted from the frequency domain, which include valuable information and are beneficial for HR image reconstruction.

In order to tackle the mentioned drawbacks and unlock more potential of Transformer for SISR, we propose a novel architecture named Channel-Partitioned Attention Transformer (CPAT), depicted in Fig. 1. A key component in our CPAT is the new self-attention mechanism called **Channel-Partitioned Windowed Self-Attention (CPWin-SA)** to better capture long-range information and relationships between distant tokens. In addition, we also design a **Spatial-Frequency Interaction Module (SFIM)** to integrate the spatial and frequency domains to fully exploit the information from feature maps, thereby boosting the quality of output images. Based on these designs, our method can extract robust features to aid in reconstruction and achieve significant improvements compared to the current methods.

Contributions: 1) We propose a novel Channel-Partitioned Windowed Self-Attention (CPWin-SA), a robust feature extraction for better reconstruction of images. 2). We design a new Spatial-Frequency Interaction Module (SFIM) to leverage all features from both spatial and frequency domains that improve the model’s performance. 3) Our network outperforms the current state-of-the-art methods for SISR.

2 Related Work

Deep Neural Networks for SISR. Dong *et al.* [10] conducted the first study utilizing deep learning in SISR, called SRCNN, a simple yet effective three-layer CNN for SISR. Following SRCNN, CNNs have been employed in subsequent studies to enhance SISR performance [2, 30, 33, 36]. Recently, Transformer has been used in various computer vision applications, from localization [41, 52] to deeply understanding images [25, 44, 46, 58] to sequence-based networks [1, 18, 40]. ViT [16] was proposed by Dosovitskiy *et al.* that processes input images by segmenting them into patches and then projecting these patches into sequential tokens as input of transformer module and achieved remarkable results with high-level vision tasks. To reduce the high computational cost of ViT, Liu *et al.* [35] proposed a hierarchical transformer called Swin Transformer, using self-attention over local windows instead of the entire image like ViT. In the field of low-level vision tasks, such as SISR, Transformer can also be used as a powerful backbone. IPT [2] leveraged the pre-trained transformer to improve performance for the image super-resolution task. SwinIR [32] utilized Swin Transformer as a deep feature extractor and achieved impressive results for image restoration. HAT [10] proposed Hybrid Attention Transformer and Overlapping-cross Attention, achieving state-of-the-art SISR performance. However, the common limitation of these works is that they are limited in capturing long-range dependencies and may miss the connection with the distant tokens. Our proposed Transformer can handle this problem by enhancing window size in the window-based attention mechanism while still being efficient for high-resolution images.

Frequency domain in Computer Vision. The frequency domain is widely used in digital signal processing [28, 43, 49] and benefits the computer vision domain [8, 17, 20, 31], such

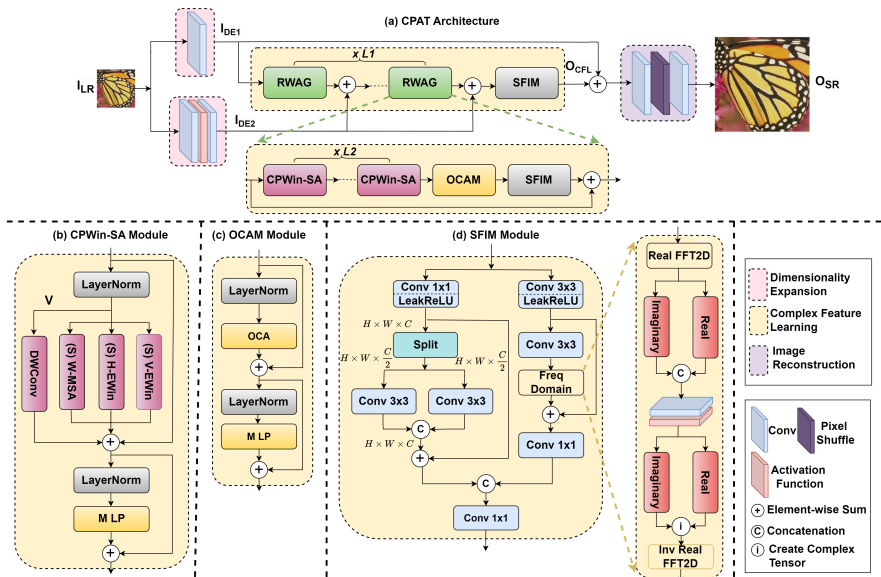


Figure 1: Architecture details. (a) The overall architecture of CPAT. (b) Structure of Channel-Partitioned Windowed Self-Attention. (c) Structure of Overlapping Cross-Attention Module. (d) Spatial-Frequency Integrated Module.

as image super-resolution. Cai *et al.* proposed FreqNet [8] consisting of two main branches: spatial and frequency branches. FreqNet transforms LR and HR images to the frequency domain using discrete cosine transform (DCT) [9]. DCT features combine with spatial features, and then, the inverse DCT (iDCT) [9] is used to convert the feature maps back to the spatial domain. FreqNet uses a dual branch and DCT transform from the beginning, which increases the computational complexity. Wang *et al.* proposed SfMNet [50] for face super-resolution (FSR). SfMNet uses Fourier transform [9] in the frequency domain to convert spatial features to the frequency domain to capture the global facial structure and inverse Fourier transform [9] to convert frequency features to the spatial domain. Similar to FreqNet, the frequency branch in SfMNet is too complex and the computational complexity is high due to it computes spatial-frequency cross-attention module multiple times to combine spatial and frequency domains. Our Spatial-Frequency Integrated Module (SFIM) is designed to deal with this problem. It is simple yet effectively leverages features (textures, edges, *etc.*) from the frequency domain that may miss extraction in the spatial domain while the computational complexity is not significantly increasing.

3 Methodology

3.1 The Overall Architecture

The overall architecture of Channel-Partitioned Attention Transformer (CPAT) is shown in Fig. 1(a), which consists of three parts: Dimensionality Expansion (DE), Complex Feature Learning (CFL), and Image Reconstruction (IR). We set the input LR and output SR images as $I_{LR} \in \mathbb{R}^{H \times W \times C_{in}}$ and $O_{SR} \in \mathbb{R}^{H \times W \times C_{out}}$, where C_{in} and C_{out} are the channel numbers of the LR and SR images, respectively. First, Dimensionality Expansion transforms I_{LR} from a

low-dimensional space to a high-dimensional space I_{DE1}, I_{DE2} as follows:

$$I_{DE1} = F_{c3}(I_{LR}), I_{DE2} = F_{c2}(I_{LR}), \quad (1)$$

where I_{DE1} and I_{DE2} are the output of DE; F_{c3} is a 3x3 conv, and F_{c2} is a convolution stage (Convolution - Activation - Convolution). Next, I_{DE1} goes through Complex Feature Learning, which involves a series of RWAGs to learn the complex and deep features. Each RWAG consists of several CPWin-SA modules, an overlapping cross-attention module (OCAM), and a SFIM module. The output of CFL O_{CFL} is

$$O_{CFL} = F_{SFIM}(F_{RWAG}^{L_1}(F_{RWAG}^{L_1-1}(\dots(F_{RWAG}^1(I_{DE1}) + I_{DE2})) + I_{DE2}) + I_{DE2}), \quad (2)$$

where F_{RWAG}^i , F_{SFIM} represent the functions of i -th RWAG, SFIM modules, $i = 1, 2, \dots, L_1$, and L_1 is the number of RWAG in CFL. Finally, O_{CFL} is passed to the Image Reconstruction (IR) to obtain the output O_{SR} . IR includes convolution layers and PixelShuffle [25]. We set the function of IR as F_{IR} , and we then have

$$O_{SR} = F_{IR}(O_{CFL} + I_{DE1}), \quad (3)$$

3.2 Channel-Partitioned Windowed Self-Attention (CPWin-SA)

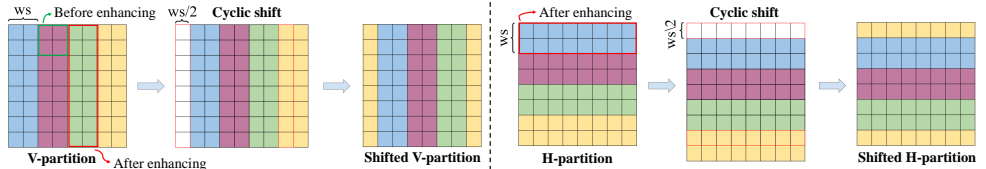


Figure 2: Enhanced window strategy and One-Direction Shift Operation in V-EWin and H-EWin

Channel-Partitioned Windowed Self-Attention (CPWin-SA) is a key component of our method, described in Fig. 1(b). It consists of three different attention mechanism types: Vertically Enhanced Window Attention (H-EWin), Horizontally Enhanced Window Attention (H-EWin), and standard Windowed Multi-head Self-Attention (W-MSA). We split the input feature maps along the channel dimension into three equal parts, corresponding to the three attentions that are above mentioned.

Enhanced Window Self-Attention. This refers to V-EWin and H-EWin. We extend the squared windows along the vertical and horizontal directions of the input feature maps, shown in Fig. 2. Specifically, the window size is extended from $ws \times ws$ (squared window) to $H \times ws$ (V-EWin) or $ws \times W$ (H-EWin), where ws is the window size ($ws < H$, $ws < W$). V-EWin and H-Ewin enhance attention areas by extending the window size, thereby increasing the ability to extract global contextual information and relationships between distant tokens. For simplicity, the mathematical descriptions below are used for V-EWin, and similar formulations can be applied to H-EWin. With the input feature $X \in \mathbb{R}^{H \times W \times \frac{C}{3}}$ (after splitting), we compute attention N times in parallel, where N is the head number. We partition X into non-overlapping windows of size $H \times ws$ for each attention head, then calculate the self-attention of the i -th window feature as $X_i \in \mathbb{R}^{H \times ws \times \frac{C}{3}}$, $i=1, \dots, \frac{H \times W}{H \times ws}$ for the n -th head,

$$Y_i^n = \text{Attention}(Q_i^n, K_i^n, V_i^n) = \text{Attention}(X_i W_n^Q, X_i W_n^K, X_i W_n^V), \quad (4)$$

where $Y_i^n \in \mathbb{R}^{H \times ws \times D}$ denotes the attention output of X_i in the n -th head, $D = \frac{C}{3N}$ represents the channel dimension in each head. $Q_i^n, K_i^n, V_i^n \in \mathbb{R}^{\frac{C}{3} \times D}$ are the projection matrices of query,

key, and value, respectively for n -th head. We use conditional position embedding (CPE) [13] to add the spatial relationships into the network. The attention feature $Y^n \in \mathbb{R}^{H \times W \times D}$ of X is obtained by calculating the attention operation on all X_i , then performing reshaping and merging them in the order of division. We then concatenate the output of all heads and combine them with a final weight matrix to achieve the attention map output of V-EWin.

$$V\text{-}EWin(x) = \text{Concat}(Y^1, \dots, Y^{N-1}, Y^N)W^p, \quad (5)$$

where the $W^p \in \mathbb{R}^{\frac{C}{3} \times \frac{C}{3}}$ denotes the projection matrix for feature fusion.

One-Direction Shift Operation. The window-based self-attention module causes a lack of information linkage between windows, thereby reducing the modeling power with distant tokens. We enhance the windows along the height and width of the feature map, we propose One-Directional Shift Operation instead of two directions as in Swin Transformer while ensuring the transformer's modeling power, detailed in Fig. 2. For V-EWin, we move the windows to the left by a distance of $\frac{ws}{2}$ pixels, while H-EWin moves downward by also $\frac{ws}{2}$ pixels. Then, we use a cyclic shift to complete the shift operation. After computing the attention operation on the shifted feature map, we then revert this feature map to obtain the feature map, which is in the original order.

Squared Window Self-Attention. For Squared Window Self-Attention, we utilize Swin Transformer (W-MSA) [33]. W-MSA is computed entirely similarly to the Enhanced Window Self-Attention we presented above. The only difference lies in the window size being $ws \times ws$ instead of $H \times ws$ or $ws \times W$. Using squared windows helps to focus on local features. Combining standard (squared) and enhanced windows and computing self-attention in various window shapes benefits datasets that contain many texture features in various directions.

Channel-Partitioned Windowed Self-Attention. CPWin-SA consists of three attention modules (V-EWin, H-EWin, and W-MSA) and an MLP, which includes a GELU [27] activation function between 2 linear projection layers. Because Transformer has no inductive bias, we simply use a depthwise convolution to add inductive bias that aims to improve the performance of Transformer. A Layer Norm layer is used before the attention modules and MLP. The entire process of CPWin-SA is as follows:

$$X = \text{LayerNorm}(X_{in}), c = C/3, \quad (6a)$$

$$X_1 = V\text{-}EWin(X[:, :, :c]), X_2 = H\text{-}EWin(X[:, :, c:2c]), X_3 = W\text{-}MSA(X[:, :, 2c:]), \quad (6b)$$

$$\hat{X} = \text{Concat}(X_1, X_2, X_3) + X_{in} + \text{DWConv}(V), \quad (6c)$$

$$X_{out} = \text{MLP}(\text{LayerNorm}(\hat{X})) + \hat{X}, \quad (6d)$$

where X_{in} , X_{out} and C are CPWin-SA's input, output features, and the channel numbers; DWConv and V are depthwise convolution and *value* matrix. Shift Operation uses two consecutive Transformer modules to increase the interaction among non-overlapping windows. The computational complexity of global MSA (self-attention is computed on the full feature map) and V-EWin are

$$\mathcal{O}(\text{Global-MSA}) = 4HW(C/3)^2 + 2(HW)^2(C/3), \quad (7a)$$

$$\mathcal{O}(V\text{-}EWin) = 4HW(C/3)^2 + 2H^2Wws(C/3), \quad (7b)$$

Assuming $H=W$ (squared image) and $ws \ll H$, $C \ll H$, the computational complexity of V-EWin is $\mathcal{O}(H^2Wws(C/3)) = \mathcal{O}(H^3)$ whereas Global-MSA is $\mathcal{O}((HW)^2(C/3)) = \mathcal{O}(H^4)$. Therefore, our proposed Transformer can be applied to high-resolution input images.

3.3 Overlapping Cross-Attention Module (OCAM)

OCAM [10] enhances the connections between windows by partitioning feature maps into overlapping windows and calculating self-attention on each window to improve the performance of the network. The structure of OCAM is depicted in Fig. 1(c). Specifically, for X_Q, X_K, X_V from the input feature X , X_Q is divided into non-overlapping windows of size $M \times M$, with $\frac{HW}{M^2}$ being the total number of windows. X_K and X_V are unfolded to $\frac{HW}{M^2}$ overlapping windows of size $M_o \times M_o$ ($M_o > M$),

$$M_o = (1 + \alpha) \times M, \quad (8)$$

where α is the overlapping ratio is 0.5. Then, self-attention is computed within each windows as in Eq. 4.

3.4 Spatial-Frequency Interaction Module (SFIM)

Spatial features may lack frequency information and fine-grained details that are important for HR image reconstruction. To address these issues, we carefully design a Spatial-Frequency Interaction Module (SFIM) shown in Fig. 1(d) to leverage the spatial and frequency domain features. SFIM consists of two branches: spatial and frequency branches. Spatial branch is helpful in extracting local spatial features. We denote the input, output of SFIM, and output of spatial as $I_{SFIM}, O_{SFIM}, O_{SB}$, respectively, then spatial branch is represented as follows:

$$O_{SB1} = F_A(F_{c1}(I_{SFIM})), \quad (9a)$$

$$O_{SB} = \text{Concat}(F_{c3}(O_{SB1}[:, :C/2, :, :]), F_{c3}(O_{SB1}[:, C/2 :, :, :]) + O_{SB1}, \quad (9b)$$

where F_{c1}, F_{c3}, F_A and C are 1x1 conv, 3x3 conv, LeakyReLU [36], and number channel, respectively. Frequency branch is used for capturing global structure and frequency information. To convert spatial features into the frequency domain, we utilize the Fast Fourier Transform (FFT) [24], and use inverse FFT (iFFT) [24] to convert frequency features back into the spatial domain. The FFT can capture global patterns, structures, and frequency information in an image that might be less apparent in the spatial domain and are essential for SR reconstruction. We denote the output of frequency branch as O_{FB} , then frequency branch can be represented as follows:

$$O_{FB1} = F_A(F_{c3}(I_{SFIM})), \quad (10a)$$

$$O_{FB} = F_{c1}(F_{FD}(F_{c3}(O_{FB1})) + O_{FB1}), \quad (10b)$$

where F_{FD} is *Freq Domain*. At the end, we combine the outputs of spatial and frequency domains to obtain the output feature of SFIM is O_{SFIM}

$$O_{SFIM} = F_{c1}(\text{Concat}([O_{SB}, O_{FB}])), \quad (11)$$

4 Experiments

4.1 Experimental Settings

We use DF2K (DIV2K [11]+Flicker2K [33]) dataset as the training set for a fair comparison with other methods. For evaluating our model, we use five benchmark datasets: Set5 [3],

Structure	PSNR	SSIM	FLOPs
Squared wins	34.03	0.9438	324.8G
Enhanced wins	34.26	0.9448	329.0G

Table 1: Effect of the enhanced windows.

Structure	PSNR	SSIM	FLOPs
w/o shift	34.13	0.9440	329.0G
w/ shift	34.26	0.9448	329.0G

Table 2: Effect of One-Direction Shift Operation.

Structure	PSNR	SSIM	FLOPs
w/o SFIM	34.14	0.9442	256.2G
w/ SFIM	34.26	0.9448	329.0G

Table 3: Effect of SFIM module.

Set14 [13], BSD100 [14], Urban100 [15], and Manga109 [16]. Furthermore, we use peak signal-to-noise ratio (PSNR) [17] and the structural similarity index measure (SSIM) [18] as quantitative metrics, which are calculated on the Y channel in YCbCr Space. For the structure of network, we set the number of RWAG and SPWin-SA to 6, the channel number to 180, and the window size is set to 16. The overlapping ratio in OCAM remains at 0.5 as in [19]. We apply the self-ensemble strategy similarly to [20] in testing that we call CPAT \dagger as in [10, 12, 13]. We use a patch size of 64×64 and a batch size of 32 during the training. We simply use L1 loss, and Adam optimizer [21] to optimize models with 500K iterations.

4.2 Ablation Study

Following [10, 12], we train x2 SR model on DF2K (DIV2K [10]+Flicker2K [13]), and test on Urban100 [15] for all experiments in this section. FLOPs are calculated on a 256x256 HR image. Results are reported in Tab. 1, 2, 3, 4, and the better results are shown in **bold**.

Effect of the enhanced window. Tab. 1 shows the effectiveness of the enhanced window in V-EWin and H-EWin instead of the squared window in Swin Transformer. PSNR, when using the enhanced window is 34.26dB compared to 34.03dB with the squared window. These results show that the standard window-based transformer has yet to fully utilize its potential for SISR, whereas our method shows significant improvement and the computation complexity does not increase much (FLOPs is 329.0G compared to 324.8G). These results also indicate that transformer-based methods remain a promising research direction in SISR.

Effect of shift operation. Tab. 2 shows the effect of One-Direction Shifted Operation. When One-Direction Shift Operation is applied, PSNR value is 34.26dB, which is higher compared to 34.13dB without this operation. Additionally, SSIM also increases from 0.9440 to 0.9448. Our shift operation is helpful in getting correlation attention between different window partitions, thereby enhancing the performance of CPWin-SA and our network in general.

Effect of SFIM. Tab. 3 shows the effectiveness of SFIM.

We replace SFIM module with a 3x3 conv (we call it "w/o SFIM") and see how it affects PSNR/SSIM. PSNR when having SFIM is 34.26dB, while PSNR when not having SFIM is 34.14dB. By leveraging information from the frequency domain, SFIM boosts the network's performance compared to using convolution only, which provides spatial features.

Structure	PSNR	SSIM	FLOPs
w/o Freq Domain	34.03	0.9434	321.4G
w/ Freq Domain	34.26	0.9448	329.0G

Table 4: Effect of Freq Domain module in SFIM

Effect of Freq Domain module on SFIM's effectiveness. To show the effectiveness of frequency features, we conduct an experiment by removing the Freq Domain module from the SFIM module. This means that the SFIM module will solely work with the spatial domain. The results are reported in Tab. 4, which is evident that SFIM operates significantly less effectively when the Freq Domain module is removed. By combining both spatial and frequency domains in the SFIM module, comprehensive features are extracted, thereby enhancing the performance of image reconstruction. Specifically, SFIM with Freq Domain achieves 34.26dB, whereas, without Freq Domain, it achieves 34.03dB. This also demonstrates the potential of combining spatial and frequency domains for other vision tasks.

Method	Scale	Set5 [3]		Set14 [3]		BSD100 [3]		Urban100 [3]		Manga109 [3]	
		PSNR	SSIM	PSNR	SSIM	PSNR	SSIM	PSNR	SSIM	PSNR	SSIM
EDSR [3]	x2	38.11	0.9601	33.92	0.9195	32.32	0.9013	32.93	0.9351	39.10	0.9773
RCAN [3]		38.27	0.9614	34.12	0.9216	32.41	0.9027	33.34	0.9384	39.44	0.9786
NLSA [3]		38.34	0.9618	34.08	0.9231	32.43	0.9027	33.42	0.9394	39.59	0.9789
ELAN [3]		38.36	0.9620	34.20	0.9228	32.45	0.9030	33.44	0.9391	39.62	0.9793
IPT* [3]		38.37	-	34.43	-	32.48	-	33.76	-	-	-
RCAN-it [3]		38.37	0.9620	34.49	0.9250	32.48	0.9034	33.62	0.9410	39.88	0.9799
SwinIR [3]		38.42	0.9623	34.46	0.9250	32.53	0.9041	33.81	0.9427	39.92	0.9797
CAT-A [3]		38.51	0.9626	34.78	0.9265	32.59	0.9047	34.26	0.9440	40.10	0.9805
DAT [3]		38.58	0.9629	34.81	0.9272	32.61	0.9051	34.37	0.9458	40.33	0.9807
HAT [3]		38.63	0.9630	34.86	0.9274	32.62	0.9053	34.45	0.9466	40.26	0.9809
CPAT (Ours)	x2	38.68	0.9633	34.91	0.9277	32.64	0.9056	34.76	0.9481	40.48	0.9814
CPAT† (Ours)		38.72	0.9635	34.97	0.9280	32.66	0.9058	34.89	0.9487	40.59	0.9816
EDSR [3]	x3	34.65	0.9280	30.52	0.8462	29.25	0.8093	28.80	0.8653	34.17	0.9476
RCAN [3]		34.74	0.9299	30.65	0.8482	29.32	0.8111	29.09	0.8702	34.44	0.9499
NLSA [3]		34.85	0.9306	30.70	0.8485	29.34	0.8117	29.25	0.8726	34.57	0.9508
ELAN [3]		34.90	0.9313	30.80	0.8504	29.38	0.8124	29.32	0.8745	34.73	0.9517
IPT* [3]		34.81	-	30.85	-	29.38	-	29.49	-	-	-
RCAN-it [3]		34.86	0.9308	30.76	0.8505	29.39	0.8125	29.38	0.8755	34.92	0.9520
SwinIR [3]		34.97	0.9318	30.93	0.8534	29.46	0.8145	29.75	0.8826	35.12	0.9537
CAT-A [3]		35.06	0.9326	31.04	0.8538	29.52	0.8160	30.12	0.8862	35.38	0.9546
DAT [3]		35.16	0.9331	31.11	0.8550	29.55	0.8169	30.18	0.8886	35.59	0.9554
HAT [3]		35.07	0.9329	31.08	0.8555	29.54	0.8167	30.23	0.8896	35.53	0.9552
CPAT (Ours)	x3	35.16	0.9334	31.15	0.8557	29.56	0.8174	30.52	0.8923	35.66	0.9559
CPAT† (Ours)		35.19	0.9335	31.19	0.8559	29.59	0.8177	30.63	0.8934	35.77	0.9563
EDSR [3]	x4	32.46	0.8968	28.80	0.7876	27.71	0.7420	26.64	0.8033	31.02	0.9148
RCAN [3]		32.63	0.9002	28.87	0.7889	27.77	0.7436	26.82	0.8087	31.22	0.9173
NLSA [3]		32.59	0.9000	28.87	0.7891	27.78	0.7444	26.96	0.8109	31.27	0.9184
ELAN [3]		32.75	0.9022	28.96	0.7914	27.83	0.7459	27.13	0.8167	31.68	0.9226
IPT* [3]		32.64	-	29.01	-	27.82	-	27.26	-	-	-
RCAN-it [3]		32.69	0.9007	28.99	0.7922	27.87	0.7459	27.16	0.8168	31.78	0.9217
SwinIR [3]		32.92	0.9044	29.09	0.7950	27.92	0.7489	27.45	0.8254	32.03	0.9260
CAT-A [3]		33.08	0.9052	29.18	0.7960	27.99	0.7510	27.89	0.8339	32.39	0.9285
DAT [3]		33.08	0.9055	29.23	0.7973	28.00	0.7515	27.87	0.8343	32.51	0.9291
HAT [3]		33.04	0.9056	29.23	0.7973	28.00	0.7517	27.97	0.8368	32.48	0.9292
CPAT (Ours)	x4	33.19	0.9069	29.34	0.7991	28.04	0.7527	28.22	0.8408	32.69	0.9309
CPAT† (Ours)		33.24	0.9071	29.36	0.7996	28.06	0.7532	28.33	0.8425	32.85	0.9318

Table 5: Quantitative comparison with state-of-the-art methods. The best, second-best, and third-best results are marked in red, blue, and green colors, respectively. “†” indicates that self-ensemble is used. IPT* [3] is trained on ImageNet.

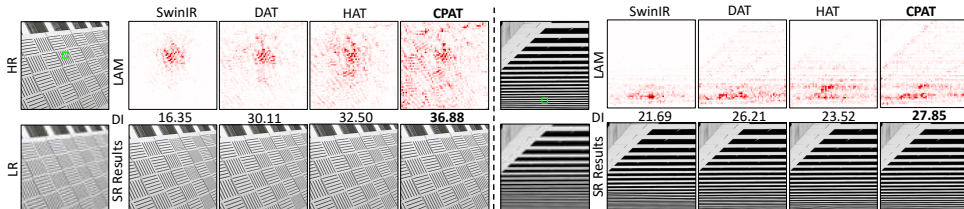


Figure 3: LAM [3] and DI [3] comparison results.

4.3 Comparison with State-of-the-Art Methods

Quantitative results. Tab. 5 reports the quantitative comparison of CPAT with different state-of-the-art methods including EDSR [33], RCAN [35], NLSA [39], ELAN [34], RCAN-it [32], SwinIR [32], CAT-A [30], DAT [30], and HAT [31]. Our method surpasses the current methods on all benchmark datasets with all scales. The highest increase achieved is 0.31dB on Urban100 on x2 SR when compared with HAT. CPAT improves by more than 0.7dB compared to SwinIR, which uses Swin Transformer as its central backbone for all scales. With the self-ensemble strategy in testing, CPAT† performs better than CPAT, but the inference time is much longer and not helpful for high-resolution input images. All

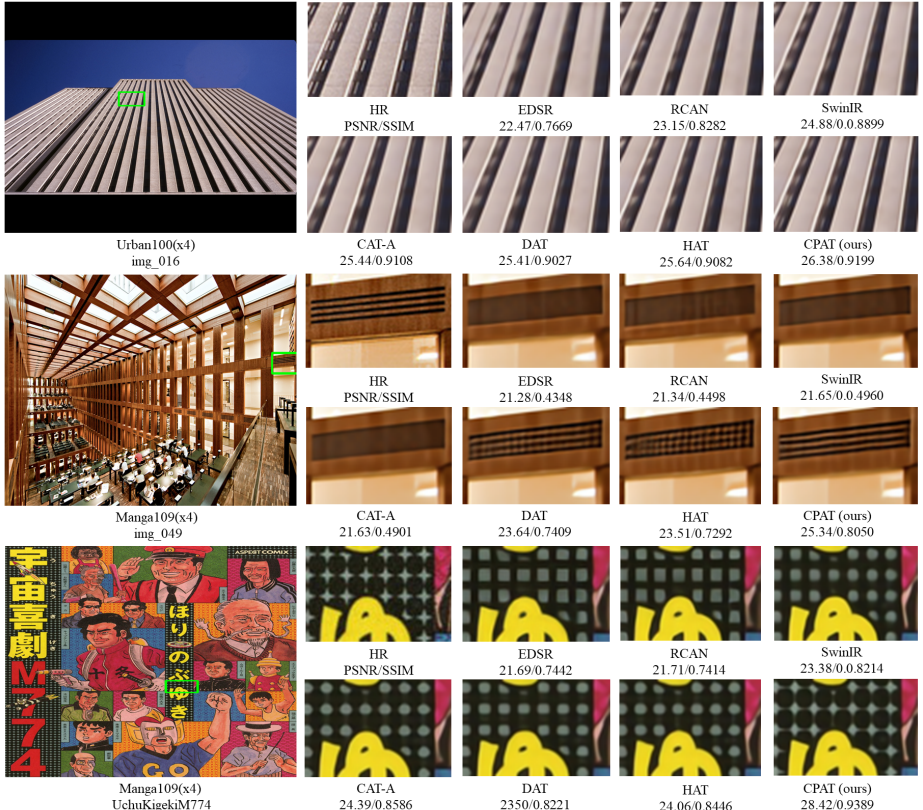


Figure 4: Qualitative comparison (x4 SR). The patch images being compared are the green boxes in the HR images. PSNR/SSIM is also computed correspondingly on these patches to demonstrate the improvement of our method.

quantitative results demonstrate that enhancing the windows along the height and width of feature maps instead of using the squared windows when computing attention in CPWin-SA and leveraging frequency features in SFIM are very effective for improving the quality of the SR image.

Qualitative results. Local Attribution Map (LAM) [19] and Diffusion Index (DI) [19] comparisons are shown in Fig. 3. LAM emphasizes the significance of pixels in the LR image during upscaling of the patches marked with green boxes. DI is indicative of the wider range of pixels utilized. A higher DI indicates a wider range of pixels in upscaling images. LAM and DI results show the superiority of our method over other methods. The visual comparison is shown in Fig. 4 with “img_16”, “img_49” from Urban100, and “UchuKigekM774” from Manga109. Our method can enhance the details of the LR image more clearly, with less blur, and higher PSNR/SSIM compared to other methods. All qualitative results show the effectiveness of our method for SISR. More details on qualitative results, self-ensemble strategy, and lightweight version of CPAT can be found in the *supp.* file.

5 Conclusions

In this study, we propose a novel Channel-Partitioned Attention Transformer (CPAT) for SISR. This Transformer consists of V-EWin, H-EWin, and W-MSA attentions. EWin and H-

EWin enhance windows along the height and width of input features to better capture long-range dependencies and relationships between distant tokens. We also use squared window-based attention in CPAT, which focuses on local features. We calculate self-attention in various window shapes to apply to datasets that contain texture features in various directions (e.g., Urban100 [2]). Additionally, we propose Spatial-Frequency Interaction Module (SFIM), which is simple yet effectively leverages features (patterns, textures, edges, *etc.*) from the frequency domain that might be less apparent in the spatial domain. Integrating frequency spatial features helps to achieve comprehensive information from feature maps that is important for HR image reconstruction. Based on the proposals above, our method outperforms the current methods in both quantitative and qualitative results.

References

- [1] E. Agustsson and R. Timofte. Ntire 2017 challenge on single image super-resolution: Dataset and study. In *2017 IEEE Conference on Computer Vision and Pattern Recognition Workshops (CVPRW)*, pages 1122–1131, Los Alamitos, CA, USA, jul 2017. IEEE Computer Society. doi: 10.1109/CVPRW.2017.150. URL <https://doi.ieee.org/10.1109/CVPRW.2017.150>.
- [2] N. Ahmed, T. Natarajan, and K.R. Rao. Discrete cosine transform. *IEEE Transactions on Computers*, C-23(1):90–93, 1974. doi: 10.1109/T-C.1974.223784.
- [3] Marco Bevilacqua, Aline Roumy, Christine M. Guillemot, and Marie-Line Alberi-Morel. Low-complexity single-image super-resolution based on nonnegative neighbor embedding. In *British Machine Vision Conference*, 2012. URL <https://api.semanticscholar.org/CorpusID:5250573>.
- [4] Théodore Bluche. Joint line segmentation and transcription for end-to-end handwritten paragraph recognition. *Advances in neural information processing systems*, 29, 2016.
- [5] E Oran Brigham. *The fast Fourier transform and its applications*. Prentice-Hall, Inc., 1988.
- [6] Runyuan Cai, Yue Ding, and Hongtao Lu. Freqnet: A frequency-domain image super-resolution network with discrete cosine transform. *ArXiv*, abs/2111.10800, 2021. URL <https://api.semanticscholar.org/CorpusID:244478402>.
- [7] Hanting Chen, Yunhe Wang, Tianyu Guo, Chang Xu, Yiping Deng, Zhenhua Liu, Siwei Ma, Chunjing Xu, Chao Xu, and Wen Gao. Pre-trained image processing transformer. In *Proceedings of the IEEE/CVF conference on computer vision and pattern recognition*, pages 12299–12310, 2021.
- [8] Jieneng Chen, Yongyi Lu, Qihang Yu, Xiangde Luo, Ehsan Adeli, Yan Wang, Le Lu, Alan L Yuille, and Yuyin Zhou. Transunet: Transformers make strong encoders for medical image segmentation. *arXiv preprint arXiv:2102.04306*, 2021.
- [9] Wuyang Chen, Xianzhi Du, Fan Yang, Lucas Beyer, Xiaohua Zhai, Tsung-Yi Lin, Huizhong Chen, Jing Li, Xiaodan Song, Zhangyang Wang, and Denny Zhou. A simple single-scale vision transformer for object detection and instance segmentation. In

Computer Vision – ECCV 2022: 17th European Conference, Tel Aviv, Israel, October 23–27, 2022, Proceedings, Part X, page 711–727, Berlin, Heidelberg, 2022. Springer-Verlag. ISBN 978-3-031-20079-3. doi: 10.1007/978-3-031-20080-9_41. URL https://doi.org/10.1007/978-3-031-20080-9_41.

- [10] Xiangyu Chen, Xintao Wang, Jiantao Zhou, Yu Qiao, and Chao Dong. Activating more pixels in image super-resolution transformer. In *Proceedings of the IEEE/CVF conference on computer vision and pattern recognition*, pages 22367–22377, 2023.
- [11] Zheng Chen, Yulun Zhang, Jinjin Gu, Linghe Kong, Xin Yuan, et al. Cross aggregation transformer for image restoration. *Advances in Neural Information Processing Systems*, 35:25478–25490, 2022.
- [12] Zheng Chen, Yulun Zhang, Jinjin Gu, Linghe Kong, Xiaokang Yang, and Fisher Yu. Dual aggregation transformer for image super-resolution. In *Proceedings of the IEEE/CVF international conference on computer vision*, pages 12312–12321, 2023.
- [13] Xiangxiang Chu, Zhi Tian, Bo Zhang, Xinlong Wang, and Chunhua Shen. Conditional positional encodings for vision transformers. In *ICLR 2023*, 2023. URL <https://openreview.net/forum?id=3KWnuT-R1bh>.
- [14] James W Cooley and John W Tukey. An algorithm for the machine calculation of complex fourier series. *Mathematics of computation*, 19(90):297–301, 1965.
- [15] Chao Dong, Chen Change Loy, Kaiming He, and Xiaoou Tang. Image super-resolution using deep convolutional networks. *IEEE transactions on pattern analysis and machine intelligence*, 38(2):295–307, 2015.
- [16] Alexey Dosovitskiy, Lucas Beyer, Alexander Kolesnikov, Dirk Weissenborn, Xiaohua Zhai, Thomas Unterthiner, Mostafa Dehghani, Matthias Minderer, Georg Heigold, Sylvain Gelly, Jakob Uszkoreit, and Neil Houlsby. An image is worth 16x16 words: Transformers for image recognition at scale. *ICLR*, 2021.
- [17] Seiichi Gohshi. Frequency domain analysis for super resolution image reconstruction and its limitations. In *2015 10th Asia-Pacific Symposium on Information and Telecommunication Technologies (APSITT)*, pages 1–3, 2015. doi: 10.1109/APSITT.2015.7217088.
- [18] Daria Grechishnikova. Transformer neural network for protein specific de novo drug generation as machine translation problem. *bioRxiv*, 2019. doi: 10.1101/863415. URL <https://www.biorxiv.org/content/early/2019/12/03/863415>.
- [19] Jinjin Gu and Chao Dong. Interpreting super-resolution networks with local attribution maps. In *Proceedings of the IEEE/CVF Conference on Computer Vision and Pattern Recognition*, pages 9199–9208, 2021.
- [20] Chao He, Zhenxue Chen, and Chengyun Liu. Salient object detection via images frequency domain analyzing. *Signal, Image and Video Processing*, 10:1295–1302, 2016.
- [21] Sen He, Wentong Liao, Hamed R Tavakoli, Michael Yang, Bodo Rosenhahn, and Nicolas Pugeault. Image captioning through image transformer. In *Proceedings of the Asian conference on computer vision*, 2020.

- [22] Dan Hendrycks and Kevin Gimpel. Gaussian error linear units (gelus). *arXiv preprint arXiv:1606.08415*, 2016.
- [23] Jia-Bin Huang, Abhishek Singh, and Narendra Ahuja. Single image super-resolution from transformed self-exemplars. In *2015 IEEE Conference on Computer Vision and Pattern Recognition (CVPR)*, pages 5197–5206, 2015. doi: 10.1109/CVPR.2015.7299156.
- [24] Z. Huang, X. Wang, Y. Wei, L. Huang, H. Shi, W. Liu, and T. S. Huang. Ccnet: Criss-cross attention for semantic segmentation. *IEEE Transactions on Pattern Analysis & Machine Intelligence*, 45(06):6896–6908, jun 2023. ISSN 1939-3539. doi: 10.1109/TPAMI.2020.3007032.
- [25] Max Jaderberg, Karen Simonyan, Andrew Zisserman, et al. Spatial transformer networks. *Advances in neural information processing systems*, 28, 2015.
- [26] Jiwon Kim, Jung Kwon Lee, and Kyoung Mu Lee. Accurate image super-resolution using very deep convolutional networks. In *Proceedings of the IEEE conference on computer vision and pattern recognition*, pages 1646–1654, 2016.
- [27] Jiwon Kim, Jung Kwon Lee, and Kyoung Mu Lee. Deeply-recursive convolutional network for image super-resolution. In *Proceedings of the IEEE conference on computer vision and pattern recognition*, pages 1637–1645, 2016.
- [28] JM Kim, SH Kim, DJ Lee, and HS Lim. Signal processing using fourier & wavelet transform for pulse oximetry. In *Technical Digest. CLEO/Pacific Rim 2001. 4th Pacific Rim Conference on Lasers and Electro-Optics (Cat. No. 01TH8557)*, volume 2, pages II–II. IEEE, 2001.
- [29] Diederik P. Kingma and Jimmy Ba. Adam: A method for stochastic optimization. *CoRR*, abs/1412.6980, 2014. URL <https://api.semanticscholar.org/CorpusID:6628106>.
- [30] Christian Ledig, Lucas Theis, Ferenc Huszár, Jose Caballero, Andrew Cunningham, Alejandro Acosta, Andrew Aitken, Alykhan Tejani, Johannes Totz, Zehan Wang, et al. Photo-realistic single image super-resolution using a generative adversarial network. In *Proceedings of the IEEE conference on computer vision and pattern recognition*, pages 4681–4690, 2017.
- [31] Juncheng Li, Faming Fang, Kangfu Mei, and Guixu Zhang. Multi-scale residual network for image super-resolution. In *Proceedings of the European Conference on Computer Vision (ECCV)*, September 2018.
- [32] Jingyun Liang, Jiezhang Cao, Guolei Sun, Kai Zhang, Luc Van Gool, and Radu Timofte. Swinir: Image restoration using swin transformer. In *Proceedings of the IEEE/CVF international conference on computer vision*, pages 1833–1844, 2021.
- [33] Bee Lim, Sanghyun Son, Heewon Kim, Seungjun Nah, and Kyoung Mu Lee. Enhanced deep residual networks for single image super-resolution. In *Proceedings of the IEEE conference on computer vision and pattern recognition workshops*, pages 136–144, 2017.

- [34] Zudi Lin, Prateek Garg, Atmadeep Banerjee, Salma Abdel Magid, Deqing Sun, Yulun Zhang, Luc Van Gool, Donglai Wei, and Hanspeter Pfister. Revisiting rcan: Improved training for image super-resolution. *arXiv preprint arXiv:2201.11279*, 2022.
- [35] Ze Liu, Yutong Lin, Yue Cao, Han Hu, Yixuan Wei, Zheng Zhang, Stephen Lin, and Baining Guo. Swin transformer: Hierarchical vision transformer using shifted windows. In *Proceedings of the IEEE/CVF international conference on computer vision*, pages 10012–10022, 2021.
- [36] Andrew L Maas, Awni Y Hannun, Andrew Y Ng, et al. Rectifier nonlinearities improve neural network acoustic models. In *Proc. icml*, volume 30, page 3. Atlanta, GA, 2013.
- [37] D. Martin, C. Fowlkes, D. Tal, and J. Malik. A database of human segmented natural images and its application to evaluating segmentation algorithms and measuring ecological statistics. In *Proceedings Eighth IEEE International Conference on Computer Vision. ICCV 2001*, volume 2, pages 416–423 vol.2, 2001. doi: 10.1109/ICCV.2001.937655.
- [38] Yusuke Matsui, Kota Ito, Yuji Aramaki, Azuma Fujimoto, Toru Ogawa, Toshihiko Yamasaki, and Kiyoharu Aizawa. Sketch-based manga retrieval using manga109 dataset. *Multimedia Tools and Applications*, 76(20):21811–21838, November 2016. ISSN 1573-7721. doi: 10.1007/s11042-016-4020-z. URL <http://dx.doi.org/10.1007/s11042-016-4020-z>.
- [39] Yiqun Mei, Yuchen Fan, and Yuqian Zhou. Image super-resolution with non-local sparse attention. In *2021 IEEE/CVF Conference on Computer Vision and Pattern Recognition (CVPR)*, pages 3516–3525, 2021. doi: 10.1109/CVPR46437.2021.00352.
- [40] Antoine Miech, Ivan Laptev, and Josef Sivic. Learnable pooling with context gating for video classification. *arXiv:1706.06905*, 2017.
- [41] Sai Saketh Rambhatla, Ishan Misra, Rama Chellappa, and Abhinav Shrivastava. Most: Multiple object localization with self-supervised transformers for object discovery. In *Proceedings of the IEEE/CVF International Conference on Computer Vision*, pages 15823–15834, 2023.
- [42] Kyle Sargent, Jing Yu Koh, Han Zhang, Huiwen Chang, Charles Herrmann, Pratul Srinivasan, Jiajun Wu, and Deqing Sun. Vq3d: Learning a 3d-aware generative model on imagenet. In *Proceedings of the IEEE/CVF International Conference on Computer Vision*, pages 4240–4250, 2023.
- [43] Rajiv Saxena and Kulbir Singh. Fractional fourier transform: A novel tool for signal processing. *Journal of the Indian Institute of Science*, 85(1):11, 2005.
- [44] Shaoshuai Shi, Li Jiang, Dengxin Dai, and Bernt Schiele. Motion transformer with global intention localization and local movement refinement. *Advances in Neural Information Processing Systems*, 35:6531–6543, 2022.
- [45] W. Shi, J. Caballero, F. Huszar, J. Totz, A. P. Aitken, R. Bishop, D. Rueckert, and Z. Wang. Real-time single image and video super-resolution using an efficient sub-pixel convolutional neural network. In *2016 IEEE Conference on Computer Vision and Pattern Recognition (CVPR)*, pages 1874–1883, Los Alamitos, CA, USA,

jun 2016. IEEE Computer Society. doi: 10.1109/CVPR.2016.207. URL <https://doi.ieeecomputersociety.org/10.1109/CVPR.2016.207>.

[46] Jiankai Sun, Bolei Zhou, Michael J Black, and Arjun Chandrasekaran. Locate: End-to-end localization of actions in 3d with transformers. *arXiv preprint arXiv:2203.10719*, 2022.

[47] Radu Timofte, Rasmus Rothe, and Luc Van Gool. Seven ways to improve example-based single image super resolution. In *Proceedings of the IEEE conference on computer vision and pattern recognition*, pages 1865–1873, 2016.

[48] Dinh-Phu Tran, Quoc-Anh Nguyen, Van-Truong Pham, and Thi-Thao Tran. Trans2unet: Neural fusion for nuclei semantic segmentation. In *11th International Conference on Control, Automation and Information Sciences, ICCAIS 2022, Hanoi, Vietnam, November 21-24, 2022*, pages 583–588. IEEE, 2022. doi: 10.1109/ICCAIS56082.2022.9990159. URL <https://doi.org/10.1109/ICCAIS56082.2022.9990159>.

[49] R Trider. A fast fourier transform (fft) based sonar signal processor. *IEEE Transactions on Acoustics, Speech, and Signal Processing*, 26(1):15–20, 1978.

[50] Chenyang Wang, Junjun Jiang, Zhiwei Zhong, and Xianming Liu. Spatial-frequency mutual learning for face super-resolution. In *Proceedings of the IEEE/CVF Conference on Computer Vision and Pattern Recognition (CVPR)*, pages 22356–22366, June 2023.

[51] Yiyu Wang, Jungang Xu, and Yingfei Sun. End-to-end transformer based model for image captioning. In *Proceedings of the AAAI Conference on Artificial Intelligence*, volume 36, pages 2585–2594, 2022.

[52] Zhou Wang, Alan C Bovik, Hamid R Sheikh, and Eero P Simoncelli. Image quality assessment: from error visibility to structural similarity. *IEEE transactions on image processing*, 13(4):600–612, 2004.

[53] Roman Zeyde, Michael Elad, and Matan Protter. On single image scale-up using sparse-representations. volume 6920, pages 711–730, 06 2010. ISBN 978-3-642-27412-1. doi: 10.1007/978-3-642-27413-8_47.

[54] Xindong Zhang, Hui Zeng, Shi Guo, and Lei Zhang. Efficient long-range attention network for image super-resolution. In *European conference on computer vision*, pages 649–667. Springer, 2022.

[55] Yulun Zhang, Kunpeng Li, Kai Li, Lichen Wang, Bineng Zhong, and Yun Fu. Image super-resolution using very deep residual channel attention networks. In *Proceedings of the European conference on computer vision (ECCV)*, pages 286–301, 2018.

[56] Yulun Zhang, Yapeng Tian, Yu Kong, Bineng Zhong, and Yun Fu. Residual dense network for image super-resolution. In *Proceedings of the IEEE conference on computer vision and pattern recognition*, pages 2472–2481, 2018.

[57] Fang Zhao, Jianshu Li, Jian Zhao, and Jiashi Feng. Weakly supervised phrase localization with multi-scale anchored transformer network. In *Proceedings of the IEEE Conference on Computer Vision and Pattern Recognition*, pages 5696–5705, 2018.

[58] Sijie Zhu, Mubarak Shah, and Chen Chen. Transgeo: Transformer is all you need for cross-view image geo-localization. In *Proceedings of the IEEE/CVF Conference on Computer Vision and Pattern Recognition*, pages 1162–1171, 2022.